https://doi.org/10.1590/jatm.v13.1214 ORIGINAL PAPER

Computational Aerodynamics Study of Competing Conceptual Designs for Advanced Tactical Fighter Aircraft

Waseeq Siddiqui[1], Hassan Naseer[1], Syed Mohsin Zahid[1], Adnan Maqsood[1,*], Shuaib Salamat[2], Rizwan Riaz[1]

1. National University of Sciences & Technology – Research Center for Modeling & Simulation – Computational Aeronautics Laboratory – Islamabad – Pakistan. 2. National University of Sciences & Technology – College of Aeronautical Engineering – Risalpur – Pakistan.
*Correspondence author: adnan@rcms.nust.edu.pk

ABSTRACT

Advanced tactical fighter (ATF) configurations are bound to perform high angle of attack (AoA) maneuvers. However, existing conceptual design tools available in aerospace industry are based on empirical or potential flows that cannot predict aerodynamic data in nonlinear regimes. High-fidelity computational fluid dynamics algorithms have to be incorporated during conceptual design phase for better assessment between competing configurations. In this research, steady state aerodynamic analysis is conducted to compare four conceptual designs of advanced tactical fighters through Reynolds-averaged Navier–Stokes (RANS) simulations. Prior to the study, two validation test cases were conducted based on ONERA M6 Wing and benchmark unmanned combat air vehicle (UCAV) design to assess the computational setup for the problem. Pressure based solver is used to model the flow field in subsonic, transonic and supersonic regimes at sea level for all four competing designs. The quantitative results include the aerodynamic forces and the longitudinal stability coefficient comparisons among the models and its components. The qualitative analyses include pressure distribution, eddy shedding and behavior of vortices at varying flow angle. Additionally, the empirical estimation for interpolation and post-stall extrapolation are carried out for further flight performance studies.

Keywords: Aircraft configurations; Static aerodynamic characteristic; Pitching moments.

INTRODUCTION

The conceptual stage of the aircraft design focuses on the efficient evaluation of various configurations. Due to time constraints, the experimental analysis in the form of flight and wind tunnel testing are not done at this stage. It takes considerable amount of time to construct a scaled down model that is geometrically similar to the intended configuration. Moreover, there is a significant experiment set up time that is not feasible for large volumes of configurations. Even when the testing begins, the probes, the wall and the sting effects affect the flow field that needs iterative corrections to eliminate interferences. Therefore, the analytical and computational tools are put to use for the rapid evaluation of the best performer in a series of different concepts economically. The linear regime of aerodynamics is studied mainly using empirical and linearized computer codes, which include the vortex lattice method (VLM), the potential flow theory and the lifting line theory (Schminder 2012; Amadori *et al.* 2008).

Received: Sept. 23 2020 | **Accepted:** Feb. 03 2021
Peer Review History: Double Blind Peer Review.
Section Editor: Paulo Greco

The nonlinear phenomenon, which include the dominating viscous effects, are estimated using the codes VORSTAB (Tseng and Lan 1988) and DATCOM (Williams and Vukelich 1979). The VORSTAB code, which is based on the modifications to the potential flow theory, generates good estimates of stability coefficients that are in reasonable agreement with wind tunnel results. However, the code would provide successful prediction only when accurate inputs are provided, which include the geometrical representation of the model and the predicted location of the vortex lift. DATCOM, developed by United States Air Force (USAF) can provide rapid aerodynamic and stability assessment of simple shapes. The tool provides credible predictions of simple geometry over wide range of angles of attack (AoA), such as a body fin configuration (Abney and McDaniel 2005), but cannot estimate the aerodynamics of complex geometries and in transonic regime (Williams and Vukelich 1979). According to Blake (1985), digital DATCOM is not able to analyze the three-surface configurations (canard, wing, horizontal tail) in a single run.

Since the modern tactical aircraft has geometrical complexities and is expected to perform complex maneuvers, computational fluid dynamics (CFD) can be used as a decent alternative to experimentation for conceptual design analysis. As evident by its versatile use in Boeing (Tinoco 1991), CFD offers the capacity to solve a range of complicated flow problems where the empirical approach is inadequate, such as vortex dominated flows at high AoA. In the past, CFD faced several challenges in the conceptual design stage. The accuracy of the geometry in consideration was a major challenge for the designers. The absence of baseline for validation in the conceptual stage was an additional issue. Several aerodynamic performance indicators could not be assessed, such as the percentage of maximum leading-edge suction. These limitations created risks, especially for configurations that were designed to enter nonlinear flight regimes frequently (Mason *et al.* 1998). In addition, the computational cost and time of the CFD analysis was another concern. A lot of computational effort was required to perform meshing and simulation on one design. Today, the time of the cycle has decreased due to the evolution of the computing capacity and automated mesh generation algorithms. However, the amount of work needed in conventional conceptual design studies is still sufficiently high. Nevertheless, researchers and designers have started to rely on CFD for multidimensional problems due to rapidly increasing computational resources.

The Reynolds-averaged Navier–Stokes (RANS) based formulation has been widely used to study the external flow over aircraft shapes. Xue *et al.* (2016) investigated the characteristics of forward and backward sweep wings on aerodynamic characteristics. Zhong and Zhao (2012) learned the influence of engine nacelles and strakes on the maximum lift, the stall angle and the airflow around civil aircraft at high angle of attack (AoA). For a light aircraft configuration, Kostić *et al.* (2014) performed and compared CFD results against DATCOM and VLM. Similarly, Nicolosi *et al.* (2014) studied the aerodynamic interference due to sideslip on aircraft parts and the behavior of aerodynamic coefficients on various fuselage shapes of large turbo propeller aircraft. The evaluation of stability derivatives through CFD has also attracted appreciable attention in the past. Kryvokhatko and Masko (2017) employed the use of CFD method to study the longitudinal static stability and aerodynamic characteristics of a tube launched unmanned aerial vehicle (UAV) with variable wings rotation angles. Similarly, the static stability and neutral point was investigated in the work of Bitencourt *et al.* (2011). Schminder (2012) investigated the influence of canard and its horizontal location relative to center of gravity (CG) numerically and experimentally through wind tunnel test. It was observed that the presence of canard leads to instability of the aircraft while also changes the trim angle, elevates the maximum lift coefficient and delays stall point.

In CFD, it is essential to model or resolve turbulence. Turbulent flows are commonly calculated using RANS models. These models include SST k-ω (Menter 1994) and Spalart–Allmaras (Spalart and Allmaras 1992). While RANS is widely used for credible estimates with least computational cost, higher fidelity tools become a necessity to resolve eddies for detailed flow physics, such as aggressive flow separations. These techniques include large eddy simulation (LES), hybrid RANS-LES and the very expensive direct numerical simulation (DNS). Details on these models can be found in the Ansys Fluent Theory Guide (ANSYS 2017).

While RANS turbulence models have had a lot of success in a variety of applications, the accurate prediction of some complex flow phenomena such as 3D flow separation necessitates an experimental data or validation study to calibrate and finalize a turbulence model for an application. Della Vecchia *et al.* (2013) used the Spalart–Allmaras model to test the DLR-F11 configuration and found it to be suitable for predicting the stall point. Similarly, SST k-ω model was proven to perform best among the one and two equation eddy viscosity models for supersonic rocket aerodynamics (López *et al.* 2013).

Tactical fighter aircraft offers complicated flow physics at high AoA. Boelens (2012) studied the formation of several vortices on the X-31 aircraft for AoA greater than 12°. These vortices originated from different components of the model, which included canard, fuselage and inlet region. Recent studies (Wibowo *et al.* 2018; Sutrisno *et al.* 2019) have studied the detection of vortex phenomena. While higher fidelity tools like detached eddy simulation are widely accepted to accurately capture these complex phenomena, the model SST k-ω can fairly produce credible information about the flow as it succeeds in detecting the vortex breakdown location at higher AoA.

The present study evaluates the aerodynamic and static longitudinal stability of four different aircraft geometries using the Navier–Stokes formulation. The aerodynamic coefficients are iteratively calculated through CFD runs on a wide range of angles and flow velocities. Moreover, the post-stall stability characteristics are determined and compared among the configurations. The main objective of this research is to perform a comparative analysis of different aerodynamic configurations over the range of parameters through high fidelity simulations and develop better estimations in the conceptual phase. To optimize the design, it is essential to analyze the drag, lift and static stability trends of the fuselage, canards, wings and tails. This study also analyzes the aerodynamic characteristics of the components.

In this article, the section "Problem Formulation" covers the problem formulation, validation cases and the geometric modeling of the configurations. The quantitative and qualitative results are then discussed in the section "Results and Discussions", which includes the aerodynamic performance plots, pressure contours and flow vortices. The analytical estimations made through Polhamus method and post-stall aerodynamic predictions are also carried out. Finally, the conclusions drawn from the study are highlighted in the end.

Problem Formulation

The computational setup for this research was created by using three-dimensional RANS equations and pressure-based solver. Steady state solution was calculated using the finite volume method based commercial solver Ansys Fluent on unstructured computational grids comprising of tetrahedral, triangle, prism and pyramid elements. The comparative study of the configurations begins with the validation of test cases. Since no experimental data was available for models under consideration, some reference studies were highly necessary to validate the computational approach. Therefore, two validation studies were conducted based on a sweptback wing and an unmanned combat aerial vehicle (UCAV). Upon validation of the computational framework, four aircraft concepts were modeled and simulated. In the present research work, the grids were generated using Ansys Meshing and ICEM CFD. Numerical solution was performed in Ansys Fluent and the postprocessing of the results was performed using Tecplot, Ansys CFD post and MATLAB.

Validation Study on ONERA M6 Wing

A three-dimensional computational flow study is considered on the semispan swept wing ONERA M6 wing (Fig. 1). The test case is widely popular for validation for external flows in transonic regime. The computational domain of the model is a bullet-shaped domain composing of pressure far field surfaces and a symmetric plane. The dimensions of the domain are also presented in Fig. 1. Due to the symmetric nature of the problem, only half geometry is modeled along the XZ plane to reduce the computation time.

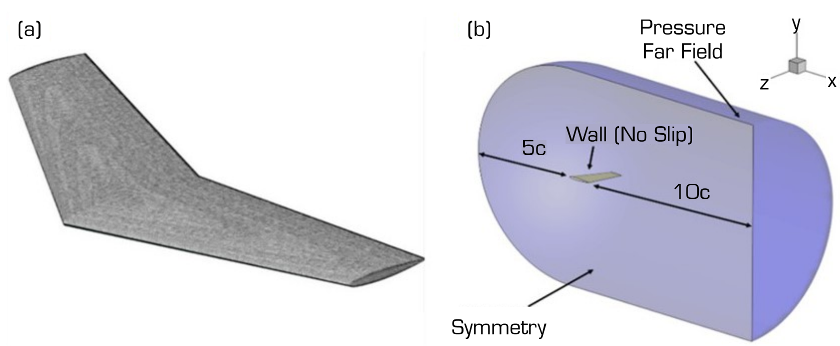

Figure 1. Computational Setup of ONERA M6 wing. (a) Geometric illustration; (b) Computational domain.

The validation test case is performed using a steady state pressure-based solver. Simple scheme is selected with least square cell based gradient and second order upwind for the remaining equations. SST k-ω is chosen as the turbulence model in this validation case under the following flow simulation conditions: Mach 0.8395, angle 3.06°, static temperature 255.56 K and gauge pressure 45.829 psi. The M6 wing is meshed using Ansys ICEM CFD and Ansys Meshing. Unstructured computational grids comprising of tetrahedral and prism volume and triangle surface elements are generated. With the expansion ratio set to 1.2, 30 inflation layers are placed and initial height is adjusted to reach y^+ below 1. The final grid sizes are 4.66 million elements for the Ansys ICEM CFD grid and 4.92 million elements for the Ansys Meshing. These grids are simulated and the numerical results are compared to the experimental data of pressure coefficient distribution from the analysis by Schmitt and Charpin (1979). The findings are plotted on different cross sections of the wing in the form of a pressure coefficient plot against the normalized chord length. As visible in Fig. 2, a good agreement between the numerical and experimental results is observed.

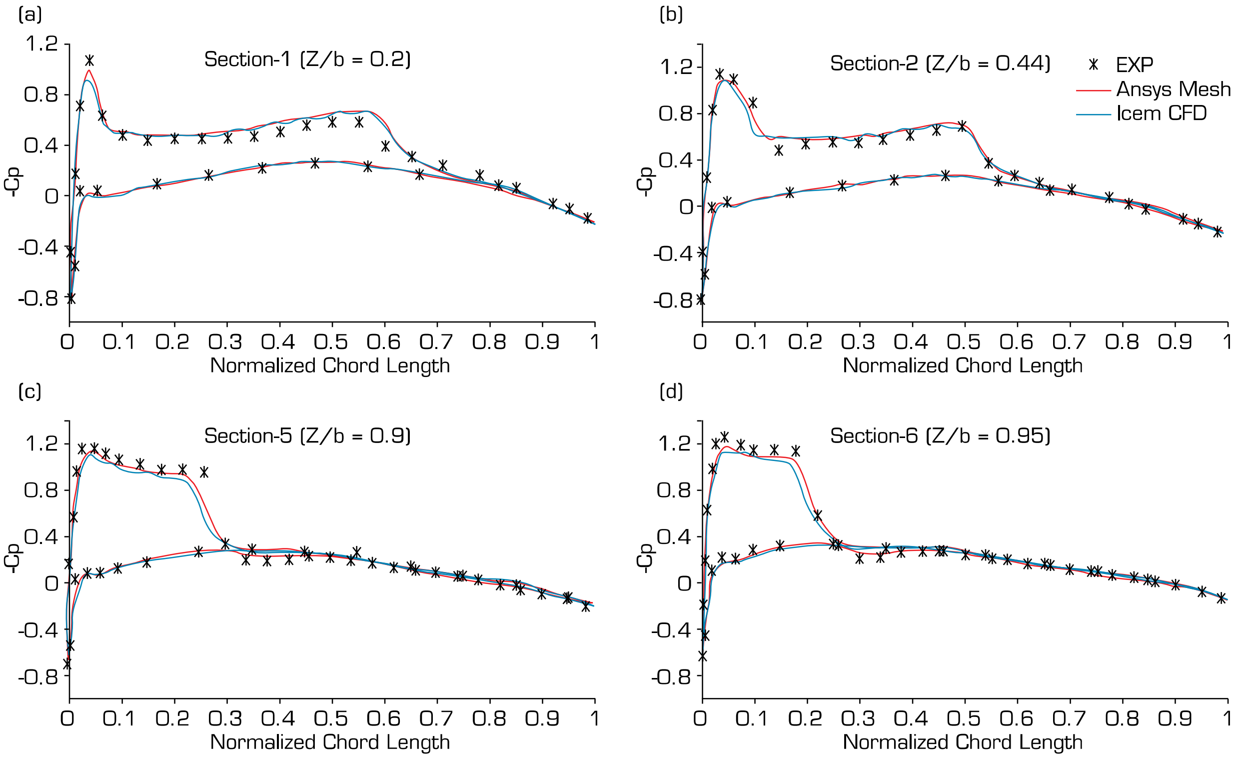

Figure 2. Pressure coefficient distribution at various sections of the wing. (a) Section 1 (Z/b = 0.2); (b) Section 2 (Z/b = 0.44); (c) Section 5 (Z/b = 0.9); (d) Section 6 (Z/b = 0.95).

Additionally, the effect of nondimensional first cell distance y^+ is investigated on the chosen turbulence model. Three different grids comprising of y^+ less than 1, less than 30 and less than 100 are investigated. It is found that the coarsest grid (y^+ less than 100) has the maximum percentage difference of 6.72% with reference to the finest grid that can be considered insignificant. Computational results for the opted range of y^+ are well coherent with experimental data allowing the flexibility of numerical grid, as can be seen in Fig. 3. However, the recommended range of y^+ for SST k-ω turbulence model is $0 < y^+ < 1$.

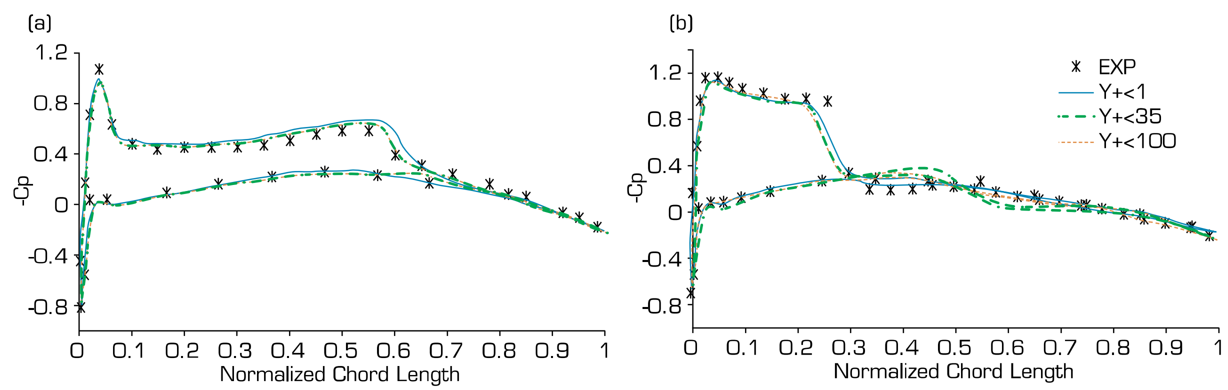

Figure 3. Influence of y^+ on pressure coefficient distribution of the wing. (a) Section 1 (Z/b = 0.2); (b) Section 5 (Z/b = 0.9).

Validation Study on UCAV

A low subsonic and incompressible fluid analysis is computationally conducted for the model UCAV. The stability and control configuration (SACCON) model was designed by the members of the AVT-161 task group on applied vehicle technology to provide a platform for static and dynamic experimental measurements, as well as for various computational simulations. With a leading-edge sweep angle of 53°, the model has a lambda wing platform. The root chord is around 1 m and the wing span is 1.53 m, while 0.479 m is the mean aerodynamic chord and 0.77 m^2 is the reference wing area (Schütte *et al.* 2009). Based on the computational and experimental work (Loeser *et al.* 2010), a geometrically similar model is constructed and simulated for assessing the credibility of the turbulence model SST k-ω.

The computational domain of the present study is similar in terms of geometrical dimensions to the previous validation test case. Since the flow is incompressible, inlet surfaces of the domain are modeled as velocity inlet, where the static temperature, flow direction and the velocity magnitude are assigned. Pressure outlet condition is imposed on the surface downstream of the wing, where atmospheric static pressure and total temperature are assigned.

The resulting grid, composing of roughly 4.5 million elements of half modeled UCAV, is simulated at sea level on a wide range of AoA. A comparison of drag coefficient C_D is plotted against the AoA in Fig. 4 between the experimental and numerical study of the present research. It can be observed that the turbulence model closely matches the experimental data till 22°. The coefficient of drag is still within 10% of the experimental work beyond 22°, which can be considered acceptable. The numerical results again match decently near 30° with the experiment. The pressure distribution on the UCAV is shown in Fig. 5.

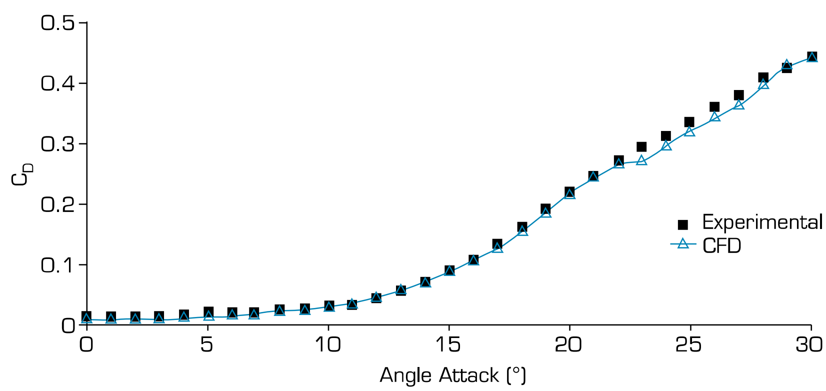

Figure 4. Comparison of C_D vs. AoA of CFD analysis with experimental data (Loeser *et al.* 2010).

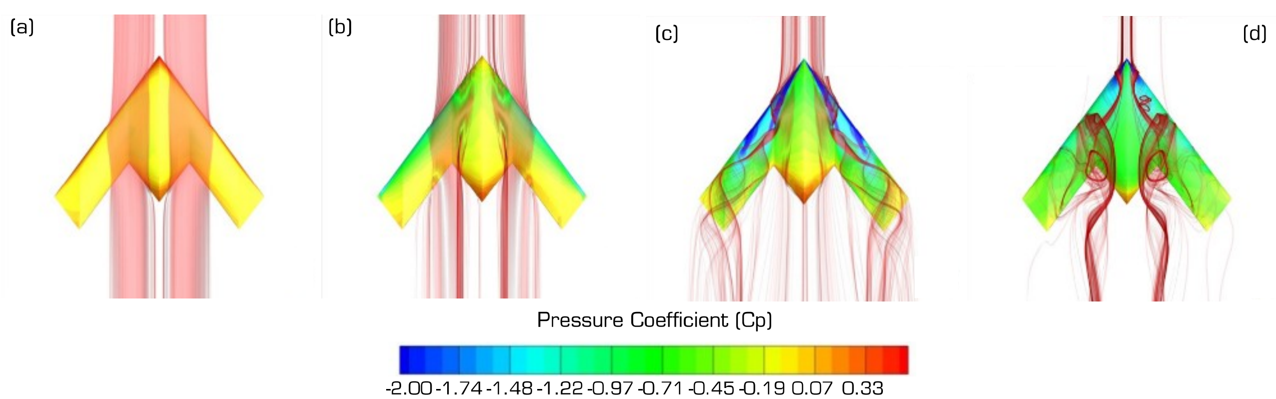

Figure 5. Flow visualization and C_p contours on upper surface of UCAV. (a) 0° AoA; (b) 10° AoA; (c) 20° AoA; (d) 30° AoA.

Modeling and Simulation of Conceptual Configurations

Computational modeling of subject study is followed by the development of accurate geometries of competing designs. Name convention for conceptual designs is set as concept-X (C-X), where X ranges from 0 to 3. Computer-aided design (CAD) models of airframes (Fig. 6) were developed in SolidWorks. Concept-0 is about V-tail idea to reduce structural weight. Concept-1 uses conventional setup of vertical and horizontal stabilizers with modified airframes. Canards are introduced in C-2 and C-3 as an effective pitch control mechanism. The geometrical dimensions are presented in Fig. 7 and Table 1.

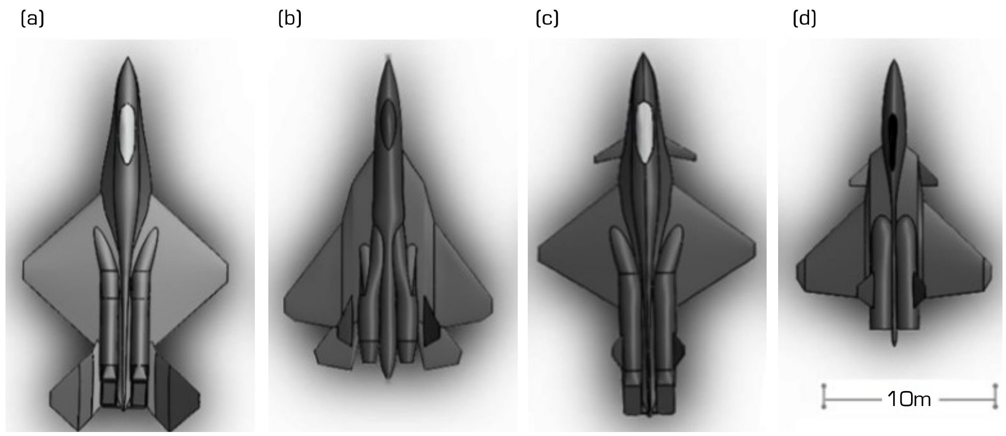

Figure 6. Computer-aided design models of all the configuration. (a) Concept-0; (b) Concept-1; (c) Concept-2; (d) Concept-3.

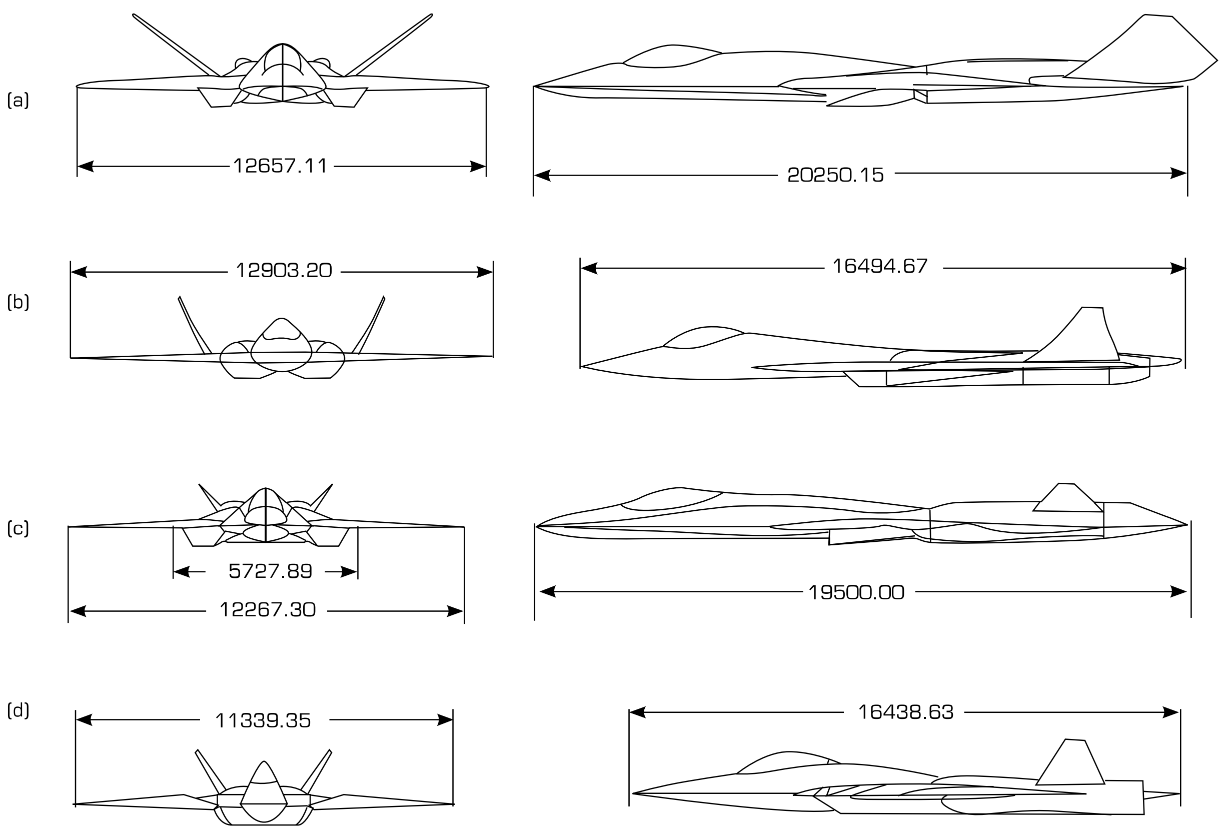

Figure 7. Geometric Dimensions of the configurations. (a) Concept-0; (b) Concept-1; (c) Concept-2; (d) Concept-3.

Table 1. Detailed dimensions of the models.

Parameters	Values/Details			
	C-0	C1	C2	C3
Fuselage Length	20.25m	18.49.	19.50m	16,44m
AircraftSpam	12.66m	12.90m	12.27m	11.34m
Aspect Ratio	2.00	2.31	2.51	2.52
Wing Leading Edge Sweep	40.00°	50.64°	34.67°	43.00°
Vertical Tail Leading Edge Sweep	47.00°	45.00°	46.65°	25.00°
Horizontal Tail Leading Edge Sweep	–	50.20°	–	–
Camard Sweep	–	–	30.00°	44.00°
Wing Airfoil	NACA 65-206	NACA 65-206	NACA 65-206	NACA 65-206
Horizontal Tail/ Canard Airfoil	NACA 0006	NACA 0006	NACA 0006	NACA 0006
Reference Area of Vertical Tail	13.83m²	8.48m²	10.12m²	5.62m²
Reference Area of Wing	80.00m²	72.00m²	60.00m²	51.00m²
Reference Area of Canard	–	–	5.06m²	2.86m²
Reference Area of HorizontalTail	–	13.20m²	–	–
Span of Horizontal Tail	–	9.14m	–	–
Span of Canard	–	–	5.73m	5.12m
Span of Wing	12.66m	12.90m	12.27m	11.34m
Mean Aerodynamic Chord of Wing	8.99m	8.03m	6.04m	7.39m
Mean Aerodynamic Chord of Horizontal Tail	–	3.86m	–	–
Mean Aerodynamic Chord of Vertical Tail	4.17m	2.08m	2.37m	1.47m
Mean Aerodynamic Chord of Canard	–	–	2.02m	1.67m
Root Chord of Wing	11.62m	10.22m	9.00m	9.37m
Root Chord of Horizontal Tail	–	2.69m	–	–
Root chord of Vertical Tail	4.34m	2.92m	2.42m	2.06m
Root Chord of Canard	–	–	1.86m	1.45m
Tip chord of Wing	1.02m	0.84m	0.76m	0.79m
Tip Chord of Horizontal Tail	–	0.80m	–	–
Tip Chord of Vertical Tail	0.80m	0.71m	0.47m	0.60m
Tip Chord of Camard	–	–	0.46m	0.33m

The concepts were modelled based on transonic area rule. Transonic area rule is an effective design technique used to reduce wave drag in transonic flight. It addresses the smooth distribution of longitudinal cross-sectional area of aircraft usually by "wasting" fuselage near wings. Longitudinal cross-sectional area distribution is presented by Fig. 8 for all the configurations. Sharp edges showing the abrupt changes in area distribution for C-0 and C-2 make these airframes more vulnerable to the formation of strong shock wave and consequent drag rise in transonic flight.

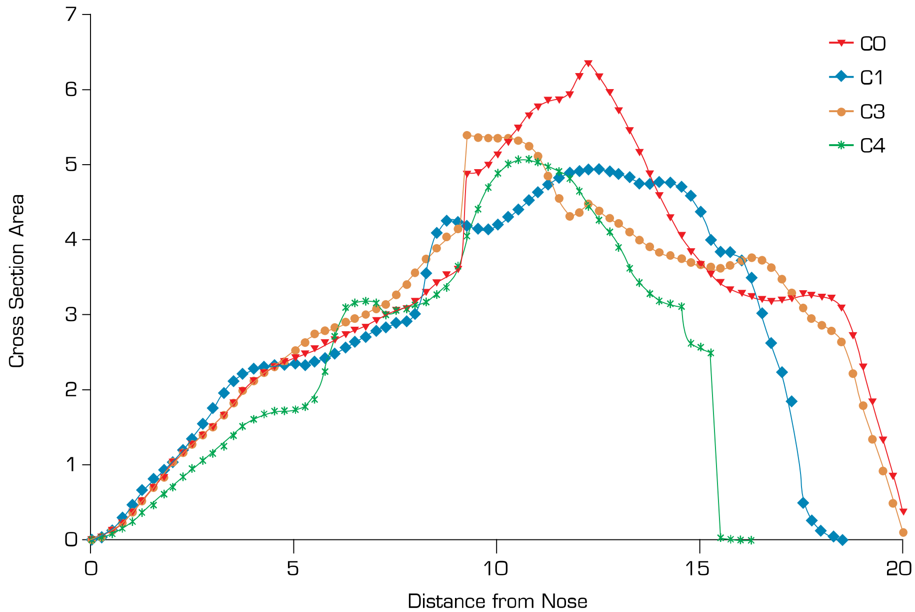

Figure 8. Longitudinal cross-sectional area distribution for area rule estimation (distance in m and area in m^2).

The preprocessing and simulation setup for the models follows the same methodology as adopted in the validation test cases. The domain for each configuration is set similarly to the validation studies (Fig. 1), where the chord would now represent the fuselage length of the aircraft. The boundary conditions are set as pressure far field for the external surfaces of the domain and symmetry condition for the symmetric plane of the domain. While the wall condition is imposed on the aircraft, the duct intake surface is assigned velocity inlet condition for subsonic stall study and no-slip condition for the remaining analysis. Fifteen layers of the nodes are placed in the boundary layer over the refined surface mesh for exhibiting average value of y^+ less than 100. The grid independence of configurations is conducted on the basis of the coefficient of drag and lift. Based on the results, similar meshing parameters are assigned to the remaining models for comparative analysis. The final grid sizes for a particular model poses 7 to 9 million elements. A representation of the volume and surface mesh is illustrated in Fig. 9.

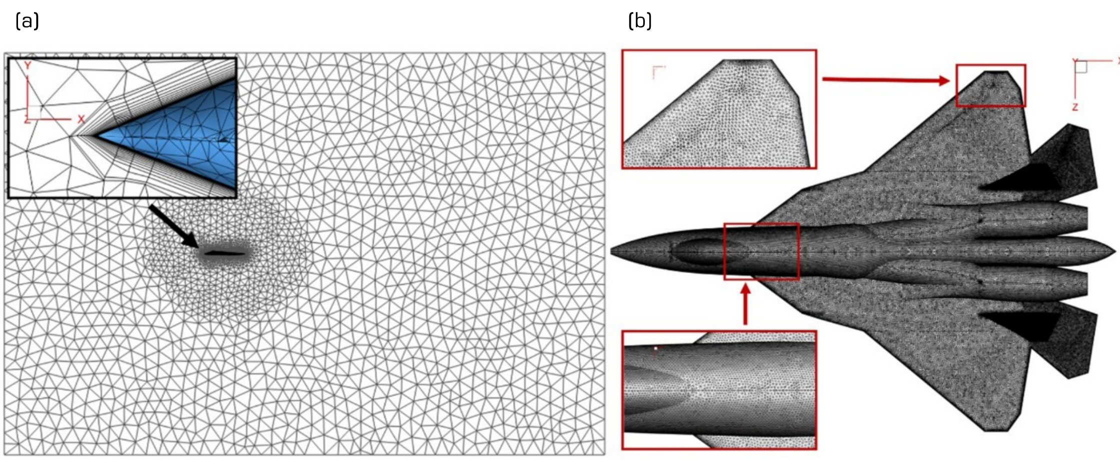

Figure 9. Meshing Topology of C-1 (a) Volume Mesh; (b) Surface Mesh.

The solution method for all simulations is set to the pressure-velocity coupled scheme. SST k-ω is employed as the turbulence model for complete analysis. The pressure, density, momentum, turbulent kinetic energy, specific dissipation rate and energy are all set to second order upwind. Viscosity is calculated using Sutherland's law and the density is set to ideal gas. The aerodynamic coefficients are monitored under the convergence criteria 10^{-6}. The grids are simulated under the flow conditions summarized in Table 2.

Table 2. Flow conditions for the study.

Altitude	Sea level
Gauge pressure (Pa)	101325.0 Pa
Static temperature	300.0 K
Subsonic Mach No.	0.6
Supersonic Mach No.	1.4
Subsonic AoA range	–10.0 to 60.0°
Supersonic AoA range	–8.0 to 20.0°
Mach range for zero-lift drag	0.2 to 2.0

Approximately 360 simulations are performed in this study. In order to accelerate the computation, parallel processing via grid partitioning and load balancing on multiple compute nodes is performed on each computational domain.

RESULTS AND DISCUSSIONS

Aerodynamic Forces and Moment Analysis

Aerodynamic evaluation is led by the comparison of basic aerodynamic coefficients, that is, the zero-lift drag coefficient C_{Do}, drag coefficient C_D, lift coefficient C_L and lift-drag ratio L/D characteristics between the competing configurations.

The zero-lift drag coefficient, C_{Do}, is an important parameter to determine the aerodynamic efficiency of the airframe. It mainly relates the wetted area of aircraft with the skin friction drag and pressure drag. Conventionally, the zero-lift drag radically increases in transonic region because of the shock wave formation. Due to its significant effect on aircraft overall size and performance, it is imperative to accurately estimate the C_{Do} even in the preliminary design stage. Figure 10 is depicting the variation in zero-lift drag coefficient at corresponding zero-lift AoA (α_0) of each conceptual design in subsonic, transonic and supersonic regimes. Concept-1 and C-2 represent the minimum and maximum value of zero-lift drag throughout the Mach range, respectively. Transonic region is highlighted in the reference Fig. 8, indicating the lowest and highest transonic drag rise for C-1 and C-2 respectively. Zero-lift drag coefficient C_{Do} vary almost alike till Mach 1 for C-0 and C-3 and rises for C-3 configuration in supersonic region. After the transonic region, drag appears to drop from maximum value in a benign manner. These observations are in coherence with the implications made through transonic area rule estimation (Fig. 8).

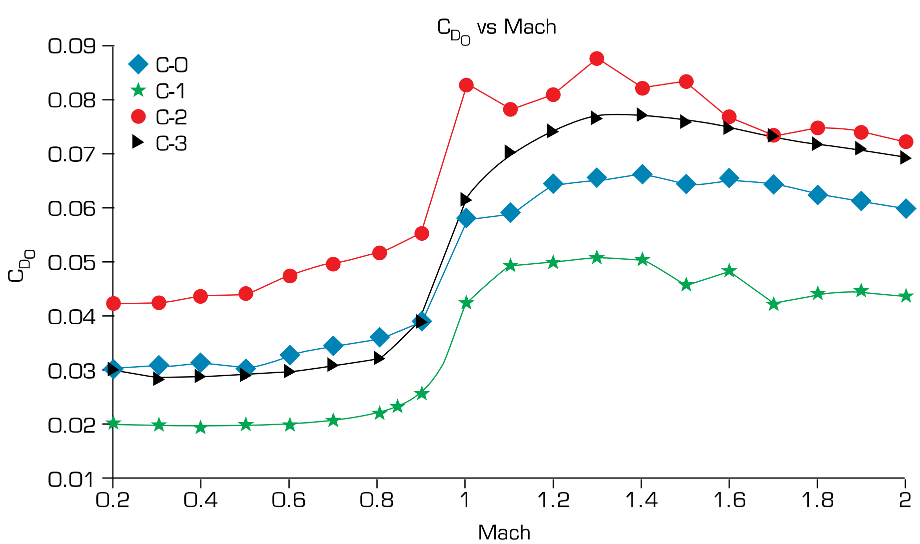

Figure 10. Zero-lift drag coefficient vs. Mach number.

Lift and drag characteristics are evaluated through their respective coefficients. Figure 11 shows the aerodynamic characteristics of concepts at subsonic and supersonic Mach. It can be observed that the lift and drag coefficients vary conventionally and are alike in the subsonic regime for all the configurations. Fairly straight slope of lift coefficient can be seen for all the configurations till 12° AoA. The highest value of lift coefficients in ascending order can be observed for C-0, C-1, C-2 and C-3 at 20° AoA. The approximate subsonic stall angle for all the configurations is 25°.

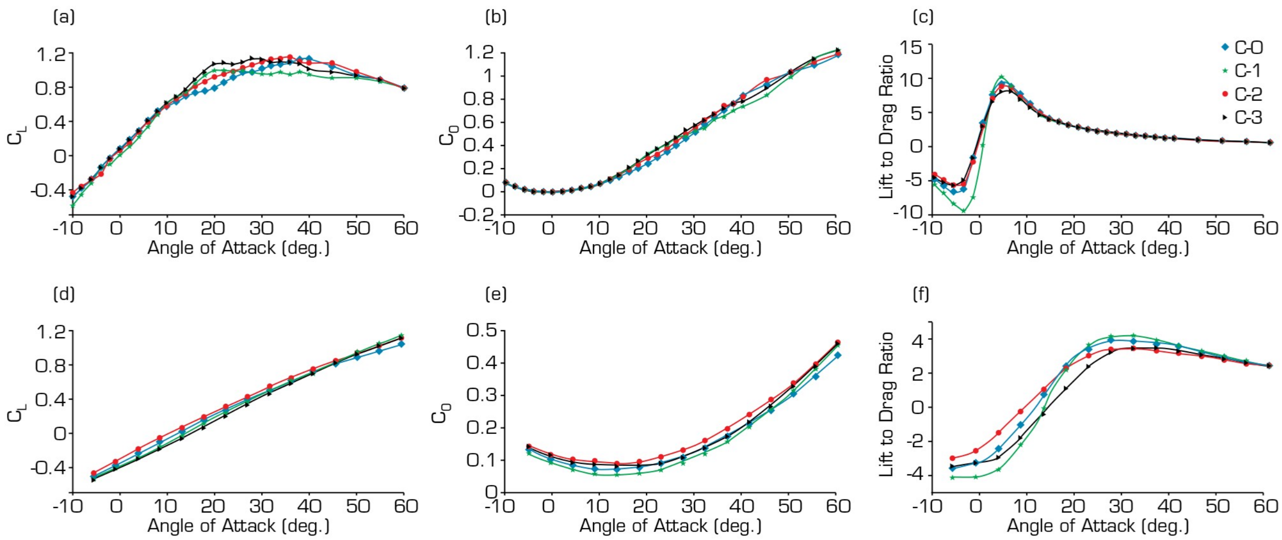

Figure 11. Comparison of aerodynamic performance at subsonic and supersonic Mach. (a) Subsonic C_L vs. AoA; (b) Subsonic C_D vs. AoA; (c) Subsonic L/D vs. AoA; (d) Supersonic C_L vs. AoA; (e) Supersonic C_D vs. AoA; (f) Supersonic L/D vs. AoA.

A flat surface behavior can be seen beyond 50° AoA. The general trend with the increasing AoA is consistent for all the airframes. Concept-2 has highest supersonic lift coefficient with the penalty of highest supersonic drag coefficient. At lower AoA, C-0 has comparatively better lift coefficient with moderate values of drag coefficient till 14° AoA. At higher AoA, highest value of supersonic lift and drag coefficients can be observed for C-1 configuration. Concept-1 has the advantage for the minimum value of supersonic drag coefficient at lower AoA, as highlighted in Fig. 11.

The overriding concern in designing the airframe is to achieve the maximum lift-to-drag ratio. The overall trend of all the configurations is consistent. The maxima of subsonic L/D for all the configurations ranges from 8 to 10, which can be observed at 4° AoA, as highlighted in Fig. 11. The maxima of supersonic L/D for all the configurations ranges from 3 to 4, which lies in between 6 and 8° AoA. Concept-1 is showing the highest lift-to-drag ratio among all the configurations in both Mach regimes.

In preliminary design study of the aircraft, one of the major stability concerns is to ensure inherited longitudinal static stability of the airframe. Pitching attitude is a key indicator to evaluate the longitudinal static stability of the aircraft. It is highly dependent on aircraft center of gravity (CG) location (X_{CG}) and determined by the pitching moment coefficient (C_m). The concept of neutral point (X_{NP}) or the location of aircraft aerodynamic center can be regarded as an alternative stability criterion. Therefore, neutral point variation study is imperative in defining the longitudinal static stability and CG positioning of the aircraft. The pitching moment coefficient at zero AoA (C_{m_o}) has to be positive to get adequate lift to balance the weight of the aircraft. The slope of C_m-alpha curve can be negative, zero or positive depending on whether X_{CG} is less than, equal to or greater than X_{NP} respectively. For the longitudinal static stability, slope of C_m-alpha curve should be negative or the location of center of gravity should lie forward of the neutral point. For quantifying the degree of static pitching stability, stick-fixed static margin is used and expressed through the formulation Eq. 1 from (Nelson 1998):

$$SM_{stick-fixed} = \frac{X_{NP}}{\bar{c}} - \frac{X_{CG}}{\bar{c}} = -\frac{C_{m\alpha}}{C_{L\alpha}} \quad (1)$$

The pitching moment coefficient at various longitudinal positions are computed to identify the neutral point of the aircraft. Center of gravity locations of each configuration, their neutral points and respective stick-fixed static margin in both subsonic and supersonic Mach regimes are tabulated in Table 3. Concept-0 is the only configuration with positive stick-fixed static margin at supersonic speed. The rest of the configurations have negative stick-fixed static margin in both Mach regimes, which implies that their CGs lie aft of the neutral point and the neutral point variation with the increasing Mach is insignificant.

Table 3. Neutral point variation and respective stick-fixed static margins of all the configurations.

Conceptual design	CG location from nose X_{cg} (m)	Neutral point from nose X_{NP} (m)		Stick-fixed static margin	
		Subsonic	Supersonic	Subsonic	Supersonic
C-0	12.06	11.08	12.50	–0.11	0.04
C-1	13.94	10.95	12.00	–0.36	–0.23
C-2	10.86	8.90	9.86	–0.19	–0.13
C-3	11.93	9.60	10.40	–0.37	–0.24

The subsonic pitching attitude at various longitudinal positions for each configuration with the behavior change in static stability experienced by shifting the location of CG is shown in Fig. 12. The displacement in the aft direction and forward direction is represented by a positive and negative sign, respectively. It is evident from the figure that all configurations are longitudinally statically unstable in subsonic regime and exhibit nonflyable value of C_{m_o} (i.e., ≤ 0). However, the overall stability is improved at supersonic speed as the neutral point shifts almost to half chord at supersonic state. Comparatively, C-0 is quite closer to the stable configuration as its C_m-alpha curves are relatively less steep. Adequately positive values of C_{m_o} for C-1 are making it fly-worthy. The rest of the configurations are almost consistent in supersonic pitching attitude.

Flow Physics

The contours of pressure coefficient (C_p) at different AoA are plotted in both subsonic and supersonic regimes at different flow angles in Fig. 13. By comparing the pressure distribution on the upper surface of the conceptual aircraft at Mach 0.6 and 8° AoA, it can be seen that the highest negative pressure is found over the leading edge of C-2 aircraft. Concept-0 has uniform pressure distribution over the wing surface. The same can also be observed over C-2 and C-3 aircraft with small span wise component. Uniformity is not maintained over the C-1, mainly due to the wing tip vortices. Concept-1 has the best pressure distribution over the blended engine nacelle, primarily due to superior fairing than other aircraft, while C-3 shows high pressure regions and thus suggests improvements for engine nacelle shape. The canards are only in C-2 and C-3 aircraft. Both canards are lifting surfaces at the given flight conditions, thus suggesting it to be effective. A negative pressure can also be seen on the V-tail in configurations C-0, C-2 and C-3. The horizontal stabilizers in C-1 configuration are also lifting and thus able to provide nominal contribution to the aircraft longitudinal stability.

As the AoA is increased to 24°, the pressure distribution across the leading edge becomes nonuniform, which is evident from Fig. 13. The main reason is the magnification of wingtip vortices generated on the lower surface of the wing, which interacts with the flow over the upper surface and thus generating a span wise velocity component. Over the leading edges, C-3 presents the best C_p distribution, followed by C-0 configuration. Concept-1 configuration seems to be affected largely by wingtip vortices that can be attributed to its double delta configuration. Concept-3 also presents the best C_p distribution over the wing surface. However, this is again undermined by the poor shape of blended nacelles, as high pressure is created at the front region (see Fig. 13). A negative pressure is maintained over the canards, and thus they are still effective at 24° AoA. In terms of efficiency, C-2 canards appear to be more efficient as compared to C-3, but the difference is very small. Concept-0 and C-1 appear to have the best pressure distribution over the vertical tail. In C-3, a high-pressure region can be seen ahead of the V-tail, thus proposing an improvement in this region. Finally, there is a negative pressure over the horizontal stabilizer of C-1, and thus it is contributing positively towards the stability of the aircraft.

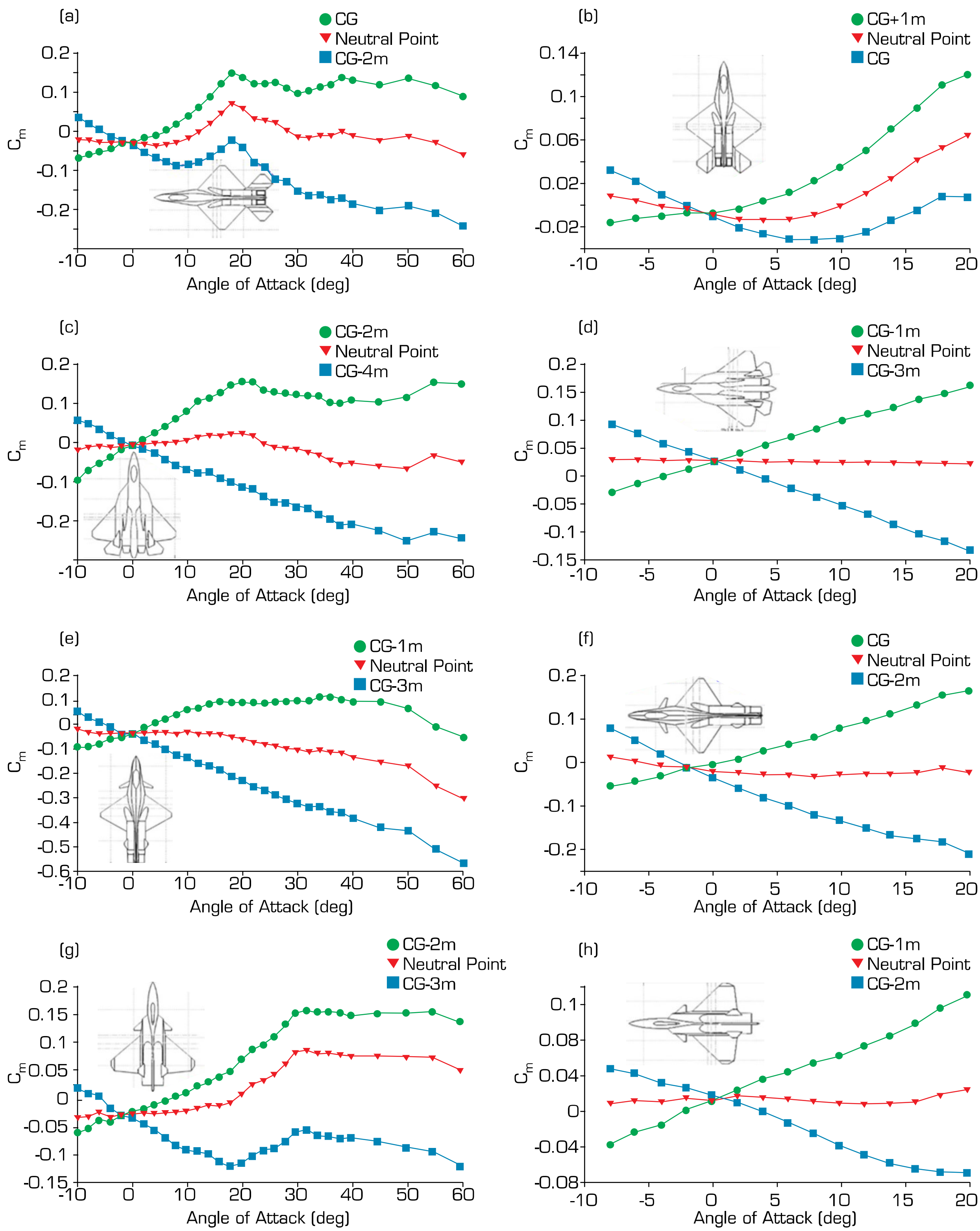

Figure 12. Pitching moment coefficient vs. AoA and Neutral Point estimation at subsonic and supersonic Mach. (a) Subsonic C_M vs. AOA for C-0; (b) Supersonic C_M vs. AOA for C-0; (c) Subsonic C_M vs. AOA for C-1; (d) Supersonic C_M vs. AOA for C-1; e) Subsonic C_M vs. AOA for C-2; (f) Supersonic C_M vs. AOA for C-2; (g) Subsonic C_M vs. AOA for C-3; (h) Supersonic C_M vs. AOA for C-3.